ACS APPLIED MATERIALS & INTERFACES

Research Article

www.acsami.org

Morphological Modification of TiO_2 Thin Films as Highly Efficient Photoanodes for Photoelectrochemical Water Splitting

Muhammad Ibadurrohman and Klaus Hellgardt*

Faculty of Engineering, Department of Chemical Engineering, Imperial College London, London SW7 2AZ, United Kingdom

Supporting Information

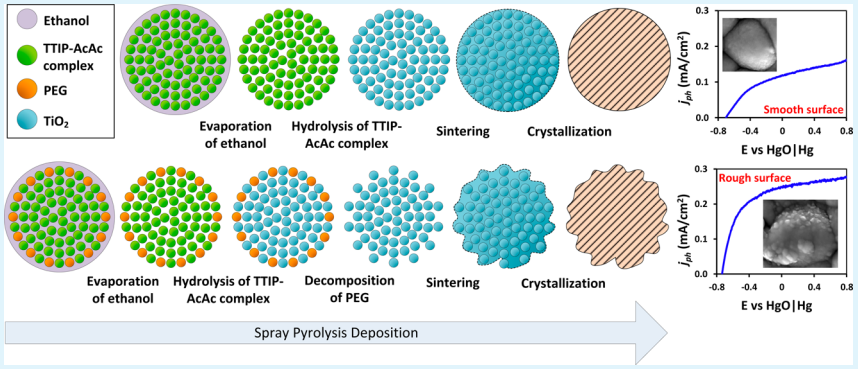

ABSTRACT: TiO_2 films with modified morphology have been successfully synthesized via a facile spray-pyrolysis method in the presence of poly(ethylene glycol) (PEG) as a templating agent. The effects of the PEG concentration on the relevant properties of TiO_2 films were investigated by means of scanning electron microscopy, X-ray diffraction, and UV−vis absorbance spectroscopy, while their photocatalytic properties were assessed by photoelectrochemical (PEC) water-splitting measurements. The introduction of 10 $g{\cdot}L^{-1}$ PEG into the precursor solution leads to surface roughening with an exceptional improvement in PEC responses, revealing a photoconversion efficiency of 1.15% at −0.50 V vs HgO|Hg (in a 1 M NaOH electrolyte under broad-spectrum illumination), which is nearly triple that of the unmodified film (0.45% at −0.38 V vs HgO|Hg). Although the efficiency of the rough-surface photoanodes deteriorates upon increasing the PEG content, their PEC responses are still superior to those of smooth-surface films. Possible phenomena that might be responsible for the experimental observations are suggested and discussed accordingly.

KEYWORDS: *TiO_2, photoanodes, poly(ethylene glycol), roughness, water splitting*

1. INTRODUCTION

H_2 has been claimed to be one of the most promising clean substitutes for fossil-based fuels, owing to its exceptional molar energy and carbon-free combustion products. Consequently, green pathways for producing H_2 have been emerging on a regular basis.[1,2] One of these pathways involves the utilization of solar energy to produce O_2 and H_2 via a water-splitting process over semiconducting materials as photon absorbers. The first successful implementation of this approach was conducted by Fujishima and Honda over 4 decades ago, employing a rutile TiO_2 single crystal as a photoanode.[3] Since then, despite possessing a large band gap, TiO_2 has been the basis of many studies in the field of solar H_2 because of its favorable thermodynamic band positions, remarkable stability, nontoxicity, and availability at reasonable price.[4]

There are two distinct systems in which semiconductor-based water photosplitting can be operable, namely, the particulate system over powdered photocatalysts and the electrode system over photoanode films.[5,6] In both systems, incident photons, with an energy level corresponding to the material band gap, induce the generation of electrons and holes in the conduction band (CB) and valence band (VB), respectively. Provided that these photocharges carry sufficient thermodynamic driving forces, they are electrochemically active to drive the evolution of H_2 and O_2. While the particulate system provides high interfacial area required for photoredox reactions, it suffers from complications regarding postoperation material recovery and gas separation.[7] On the other hand, the electrode system offers convenient material recovery and gas separation via the use of membranes, in addition to the feasibility for field bias imposition.[8] Therefore, it is arguably more desirable for long-term applications. Unfortunately, the electrode−electrolyte interfacial area is typically limited; the reaction rate is thus generally low. So, it is important to improve the real surface area of photoanode films.

Various surface architectures of semiconducting electrodes, particularly those based on TiO_2, have been introduced, including nanotubes,[9−12] nanowires,[13−15] nanorods,[16,17] and

Received: January 28, 2015
Accepted: April 13, 2015
Published: April 22, 2015

DOI: 10.1021/acsami.5b00853
ACS Appl. Mater. Interfaces 2015, 7, 9088−9097

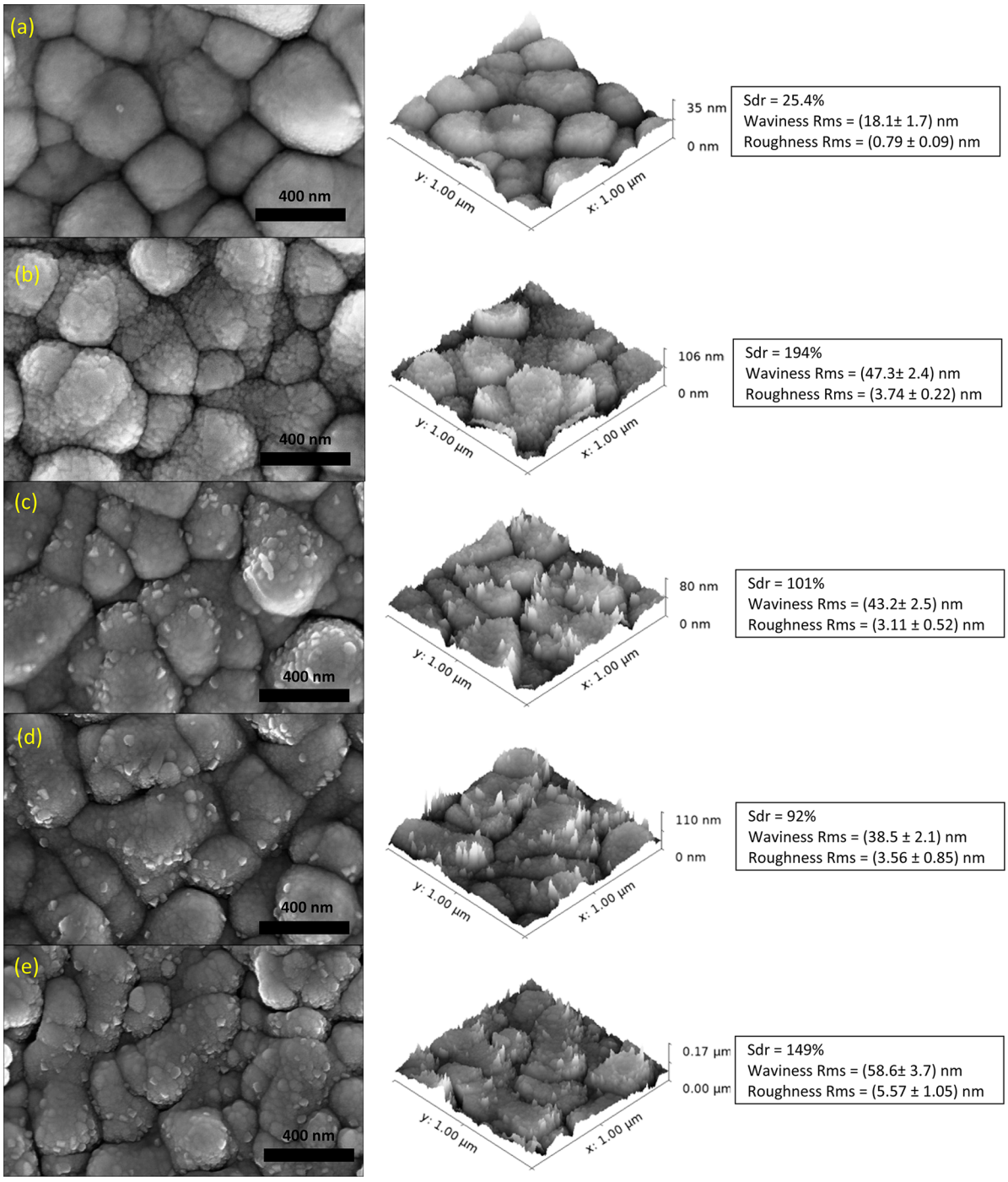

Figure 1. Top-view images of unmodified TiO_2 (a), 10PEG−TiO_2 (b), 20PEG−TiO_2 (c), 30PEG−TiO_2 (d), and 40PEG−TiO_2 (e) with their 3D views and estimated Sdr and rms values.

nanobranches.[18,19] All of these nanostructures are meant to enhance the surface-to-volume ratio of the materials and to intensify the interfacial contacts between charge carriers and their respective acceptors. Nevertheless, these nanostructures usually suffer from a low absorbed photon flux, hence lacking the photovoltage required to carry water splitting into effect.[20] Also, the characteristic thickness of these nanostructures is typically lower than the width of the space charge layer, such that the band bending is not fully developed, if any at all.[20,21] The band bending is essential for the formation of an electric field gradient, which is the driving force for the migration of electrons from the surface to the back contact, hence suppressing carrier recombination.[8] Because controlling the characteristic thickness of such nanostructures is quite a challenge, compact films are considered to be advantageous from this viewpoint because they are relatively easier to prepare with controllable thickness.

The surface area of compact films is typically improved by increasing their porosity and/or roughness via morphology modification, which can be achieved by employing templating agents. Poly(ethylene glycol) (PEG) has been renowned to be one of the best templates for the morphological alteration of TiO_2-based films.[22−25] Many synthesis routes have been reported to produce PEG-templated TiO_2 films such as sol−

DOI: 10.1021/acsami.5b00853
ACS Appl. Mater. Interfaces 2015, 7, 9088−9097

gel,[26−29] hydrothermal,[30] electrochemical anodization,[31] and spray pyrolysis.[32,33] These films have been utilized in many applications with exceptional results, such as superhydrophilic surfaces,[28,34,35] solar cells,[35] and photodegradation of pollutants.[28,36] To our knowledge, however, the use of these materials for H_2 production in photoelectrochemical (PEC) cells is rather limited. Indeed, Fei et al. have successfully synthesized PEG-templated TiO_2 films, resulting in a novel nanospider structure with an improved PEC response compared to that of the unmodified films.[37] However, the photoconversion efficiency of this film is relatively low (0.23%).

Herein, we report a significant improvement in the PEC activity by tailoring the morphology and surface roughness of TiO_2 compact films. These films were prepared via a facile and low-cost spray-pyrolysis deposition technique, employing PEG as a templating agent. The effects of this modification on the relevant properties of these films and their PEC behavior will be addressed and discussed in detail.

2. EXPERIMENTAL SECTION

Materials. The chemicals used in this study were of analytical grade and were used as received without further purification. For spray-pyrolysis deposition, titanium isopropoxide (TTIP; ≥97%, Sigma-Aldrich) was used as a TiO_2 precursor, acetylacetone (AcAc; ReagentPlus, ≥99.5%, Sigma-Aldrich) as a stabilizer, and ethanol absolute (AnalaR NORMAPUR, VWR) as a solvent. Poly(ethylene glycol) (PEG; Sigma-Aldrich) with an average molecular weight of 200 $g{\cdot}mol^{-1}$ was used as a template (morphology modifier). Fluorine-doped tin oxide (FTO; Hartford Glass Inc., USA) with a sheet resistance of 8 $\Omega{\cdot}sq^{-1}$ was used as the film underlying substrate. For PEC measurements, NaOH pellets (99.0−100.5%, AnalaR NORMAPUR, VWR) were used to prepare electrolyte solutions.

Preparation of Photoanode Films. The precursor solutions of unmodified TiO_2 films were prepared by diluting TTIP and AcAc (3:2 volumetric ratio) into 100 mL of the ethanol absolute to make 0.2 M TTIP. Subsequent ultrasonication and vigorous stirring were then applied to the prepared solutions for 0.5 and 4 h, respectively. A similar procedure was applied for the synthesis of PEG-assisted TiO_2 films, only with the addition of PEG in a concentration range of 0−40 $g{\cdot}L^{-1}$. For convenience, the PEG-assisted TiO_2 films are denoted as xPEG−TiO_2, where x is the concentration of PEG in the precursor solution in $g{\cdot}L^{-1}$. The as-prepared solutions are then subjected to spray-pyrolysis deposition, the details of which were described elsewhere.[38] Typical deposition was done for 40 layers, yet it was also varied according to necessity. All samples were then calcined at 500 °C for 2 h.

Characterization of the Films. X-ray diffractograms were recorded using a desktop D8 Bruker X-ray diffraction (XRD) machine with Cu Kα irradiation as a photon source (λ = 1.5406 Å) and a nickel filter, operating at 40 kV and 40 mA. All samples were analyzed within the range of 2θ = 5−70° at a scanning rate of ca. $2°{\cdot}min^{-1}$. The spectral absorbance of the prepared films was measured by an Agilent Technologies 8453 UV−vis spectrophotometer G1103A controlled by *ChemStation* software, with a blank FTO glass slide used as a background sample in order to eliminate the influence of spectral absorption of the substrate. The surface morphology of the prepared films was analyzed using a Zeiss LEO Gemini 1525 high-resolution field emission gun scanning electron microscope, operating at an extra high tension (EHT) of 5 kV. Open-source *Gwyddion* software was used to estimate the statistical parameters, such as the developed surface area ratio (Sdr, the increment of the surface area with respect to the projected xy plane, which is estimated by a triangulation method and would be 0% for a totally flat surface) and root-mean-square (rms) values of waviness and roughness of the prepared films, as well as to construct 3D views of the film micrographs.[39] The presented rms values were average values that are generated from 40 parallel horizontal probing lines along the y axis of scanning electron microscopy (SEM) images. The thickness of the films is evaluated by cross-sectional field emission gun scanning electron microscopic imaging. Microstructural characterization was carried out using a transmission electron microscope (JEOL 200FX) operating at 200 kV. Samples for transmission electron microscopy (TEM) analysis were obtained by removing the materials from the substrate using a razor blade.

PEC Measurements. PEC measurements were conducted in a conventional three-electrode cell with platinized titanium employed as a counter electrode and HgO|Hg (+0.926 V vs RHE) as a reference electrode. A solution of 1 M sodium hydroxide (NaOH; pH = ∼13) was used as an electrolyte. The cell was connected to a potentiostat (AUTOLAB PGSTAT302N) and controlled by *NOVA* software. A 10 $mV{\cdot}s^{-1}$ scan rate was used in all linear-sweep voltammetry measurements. A 150 W xenon lamp (LOT-Oriel GmbH & Co. KG) was used as a light source to provide broad-spectrum illumination, equipped with a TLS1509-X150 monochromator/spectrograph (Omni-λ1509, Zolix). The light intensity (ca. 125 $W{\cdot}m^{-2}$) was measured by a USB-connected StellarNet EPP2000C UV−vis spectrometer with a concave holographic grating. Typical measurements were carried out after the electrolyte solution was purged with N_2 gas for 15 min. Unless specified otherwise, all experiments were conducted at room temperature and pressure.

3. RESULTS AND DISCUSSION

Top-view micrographs of the prepared films and their corresponding 3D views are depicted in Figure 1a−e. The unmodified TiO_2 film (Figure 1a) consists of interconnected submicron aggregates with relatively smooth morphology, resulting in an Sdr value of 25.4%. It seems that the FTO underlying layer (Figure S1 in the Supporting Information, SI) acts as a template for the superstructure of our spray-pyrolyzed films. Upon the introduction of 10 $g{\cdot}L^{-1}$ PEG into the precursor solution, the roughness is evidently and uniformly enhanced across the film surface (Figure 1b), leading to a substantial enhancement in the Sdr value (194%). Upon an increase in the PEG content (Figure 1c−e), large nanosized humps are formed, although they are not uniformly distributed. This qualitative observation is corroborated by rms values calculated from 1D topographical statistics, as presented in Figure 1, signifying major development in the surface roughness upon PEG addition. Furthermore, the microstructure of TiO_2 materials is also altered significantly, as depicted in TEM images (Figure S2 in the SI). In this case, PEG plays a major role as a template that shapes the resultant morphology of the films. The disparity in thermal requirements between the evaporation of ethanol, hydrolysis of TTIP−AcAc complex, and decomposition of PEG enables subsequent events that mold the topography of the TiO_2 particles, as illustrated in Figure 2. It should be noted that Figure 2 does not specifically describe the process of particle formation along the distance between the tip of the nozzle and the preheated substrate. Because the films adhere strongly to the FTO substrate, it is likely that the particle growth was initiated after the aerosols reached the preheated substrate.

The thickness of the films was evaluated by cross-sectional SEM imaging (Figure S3a−e in the SI). The concentration of PEG has a strong influence on the film thickness, although the same 40-layer deposition was applied to all samples, as illustrated by the solid line in Figure 3a. The presence of PEG increases the portion of removable elements in the droplets. Because the spraying rate is held constant during all experiments, the mole fraction of TTIP decreases with increasing PEG content, resulting in thinner films, as described by the dashed line in Figure 3a.

DOI: 10.1021/acsami.5b00853
ACS Appl. Mater. Interfaces 2015, 7, 9088−9097

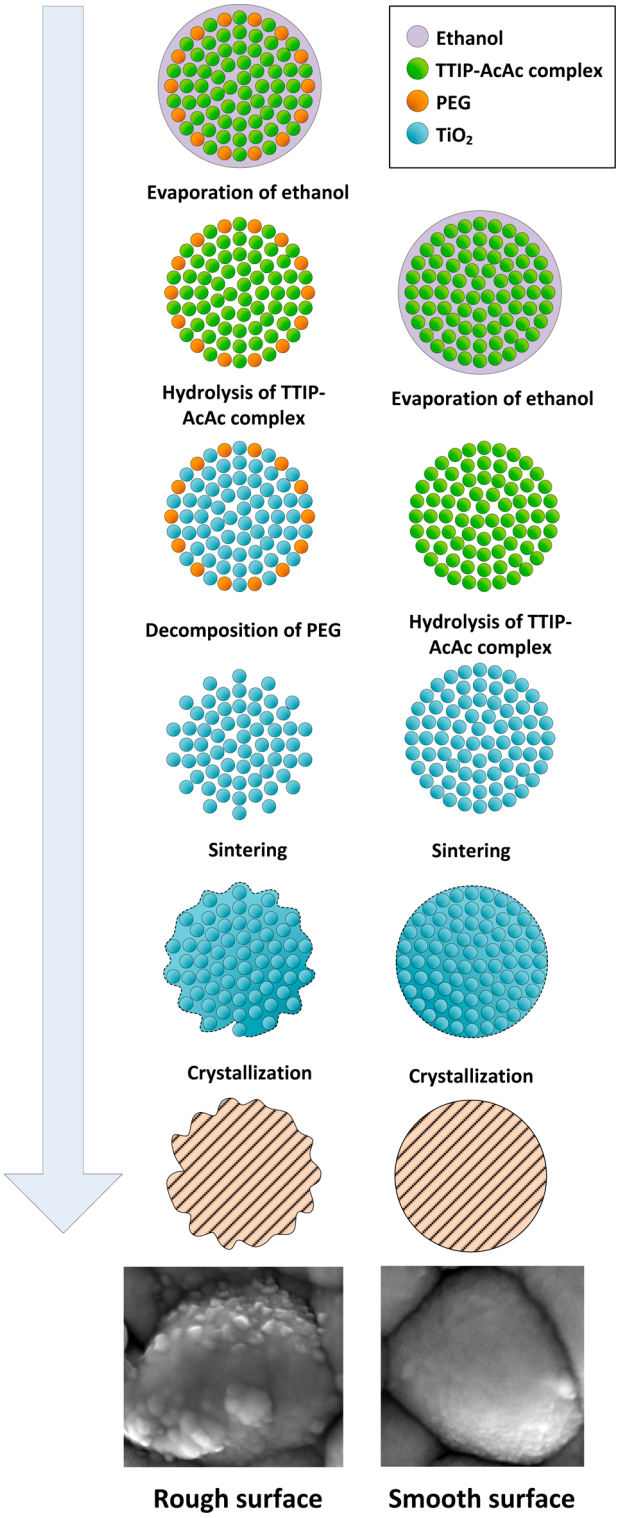

Figure 2. Illustration of the formation processes of a rough-surface film by PEG templating (a) and a smooth-surface film without PEG (b).

Figure 3b depicts the XRD patterns of the prepared film samples. The unmodified film reveals XRD characteristic peaks for the anatase crystallite phase at 2θ of 25.3° and 47.8°, which conform to the indices of the (101) and (200) planes, respectively (JCPDS card no. 21-1272). These peaks, however, gradually disappear upon the addition of PEG. This observation is attributable to a decrease in the film thickness due to PEG addition and to an increase in the grain boundaries as a result of surface roughening. Thick films are able to absorb a large quantity of heat and restrain it for a long time within their bulk regions.[40] Thus, thicker films are expected to undergo more effective heat treatments, which results in higher crystallite density as opposed to thinner films that are treated under the same conditions. Another possible postulation may also be built upon the possibility of a portion of heat that is utilized to decompose PEG during deposition and calcination. Consequently, the relative peak intensity is expected to be less developed in the case of PEG-assisted films.

Figure 4 depicts the UV−vis absorbance spectra of the prepared samples. The optical absorbance was probed at several surface points on each film and revealed essentially identical spectra (data not shown), indicating good uniformity of these films. It is clearly seen from Figure 4 that the absolute absorbance of the films decreases with an increase of the PEG concentration, particularly within the wavelength interval of 300−450 nm. This may be ascribed to variation in the film thickness. The band gap of each film is evaluated by constructing Tauc plots,[41] in which $(\alpha h\nu)^{1/2}$ is plotted against $h\nu$ according to the well-known relationship

$$(\alpha h\nu)^{1/2} = k(h\nu - E_g) \quad (1)$$

where h is the Planck constant, ν is the frequency of incident radiation, and α is the absorption coefficient calculated from the thickness-corrected absorbance, which is given by the relationship

$$\alpha = \frac{2.303A}{d} \quad (2)$$

where A is the measured absorbance and d is the film thickness in centimeters (cm). The band-gap values are obtained by extrapolating the plot of eq 1 to intercept the x axis.[41,42] Tauc plots of the prepared samples (inset of Figure 4) reveal band-gap values of 3.19, 3.20, 3.25, 3.28, and 3.30 eV for unmodified TiO_2, 10PEG−TiO_2, 20PEG−TiO_2, 30PEG−TiO_2, and 40PEG−TiO_2, respectively. The blue shifts upon surface roughening are speculated to be due to light scattering[43] and/or a significant decrease in the crystallite size,[39,44] as indicated in the XRD patterns.

Linear-sweep voltammograms of the prepared photoanode films under dark and illuminated systems are presented in Figure 5a. All samples give similar shapes of plots in which the dark scans show negligible anodic activities. The anodic photocurrent onsets occur at ca. −0.72 V vs HgO|Hg (ca. +0.2 V vs RHE) for all samples, which is in good agreement with those reported in the literature for TiO_2-based photoanodes under similar experimental conditions.[16,45,46] Beginning from these onsets, the photocurrent density immediately increases as the potential is swept toward more positive values and becomes less potential-dependent at highly positive potentials. At +0.304 V vs HgO|Hg (1.23 V vs RHE), the 10PEG−TiO_2 film gives a photocurrent density of 0.26 mA·cm^{-2}, which is 2-fold higher than that given by its unmodified counterpart (0.13 mA·cm^{-2}). Although increasing PEG concentration has a detrimental effect on PEC responses, it should be highlighted that all PEG-assisted samples still exhibit better PEC performances in comparison to their unmodified counterpart.

DOI: 10.1021/acsami.5b00853
ACS Appl. Mater. Interfaces 2015, 7, 9088−9097

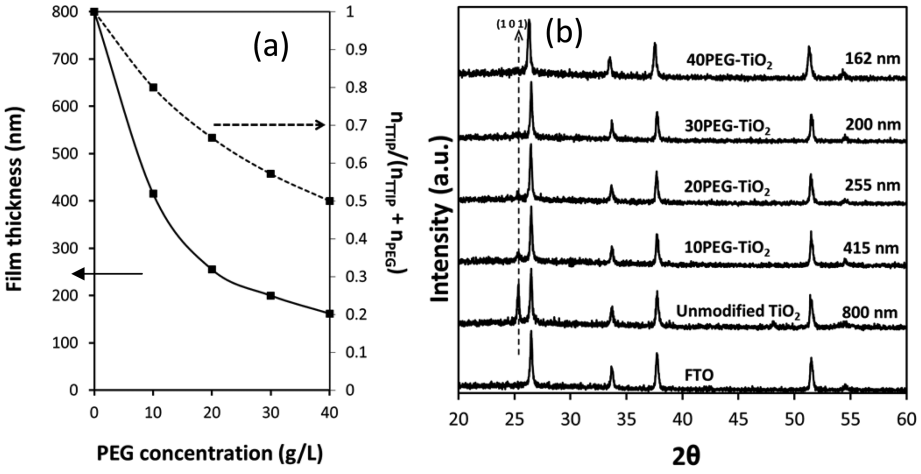

Figure 3. (a)Effect of the PEG concentration on the film thickness. (b) X-ray diffractograms of the synthesized films and their corresponding thickness.

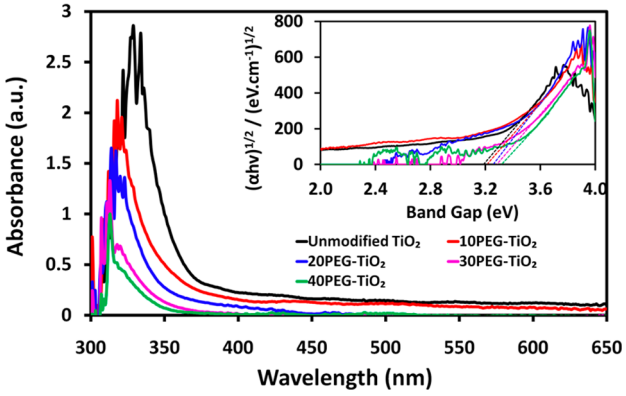

Figure 4. Spectral absorbance of the synthesized films with their corresponding Tauc plots (inset).

The linear-sweep voltammograms can be directly translated to the applied-bias photoconversion efficiency (ABPE), which is calculated by the following expression:[47]

$$\text{ABPE}\ (\%) = \frac{\text{total power output} - \text{electrical power input}}{\text{incident light power}} \times 100 \quad (3)$$

$$\text{ABPE}\ (\%) = \frac{j_p(1.23 - V)}{P} \times 100 \quad (4)$$

where j_p is the measured photocurrent density in amperes per square meter ($A{\cdot}m^{-2}$), V is the applied electrical bias with respect to RHE in volts (V), and P is the incident light power density in watts per square meter ($W{\cdot}m^{-2}$).

Figure 5b presents typical parabolic plots of ABPE as a function of the applied potential. The unmodified TiO_2 film gives a maximum ABPE of 0.45% at −0.38 V vs HgO|Hg. A remarkable improvement in ABPE is achieved by 10PEG−TiO_2, which reaches as high as 1.15% at −0.5 V vs HgO|Hg. As mentioned earlier, the PEC performance drops upon an increase in the PEG content, which results in a maximum ABPE of 0.90% at −0.42 V vs HgO|Hg, 0.76% at −0.48 V vs HgO|Hg, and 0.62% at −0.44 V vs HgO|Hg for 20PEG−TiO_2, 30PEG−TiO_2, and 40PEG−TiO_2, respectively. Therefore, it is suggested that surface modification of the films is an effective approach to boost the PEC efficiency, as well as to reduce the external bias required by the cell to reach its maximum photoconversion. Moreover, photocurrent spectra are presented in Figure 5c, in which the cutoff wavelengths correspond well with the respective band gaps of the films and the positions of the photocurrent peaks are also in agreement with the absorbance spectra.

The surface roughness of a photoanode film has a strong influence on the exposed surface area and, consequently, on the number of reactive sites.[13,46,48] The surface irregularities may also intensify the adsorption of photoelectrochemically active species, hence promoting the resultant photocurrents.[21] In addition, upon employment of rough-surface photoanodes, the nature of light absorption and carrier collection may also be enhanced in a manner illustrated in Figure 6. The incoming light is distributed more effectively via light scattering on a rough surface as opposed to that on a smooth one.[20] The presence of nanosized humps on the surface allows confinement of a large portion of reflected photons, whereas a substantial loss of absorption is expected from the use of smooth-surface films.[20] From the micrographs, it is also noticeable that the diameter of the humps is within an interval similar to the field-free diffusion length of the holes (10−70 nm).[13,46,49,50] As a result, at the same photoexcitation depth, shorter pathways for hole collection become achievable.[20] One or a combination of the aforementioned phenomena is believed to be responsible for the advanced PEC output of PEG-assisted samples.

At this point, however, one may still be in doubt as to whether enhancement in the PEC efficiency is due to an increase in the film roughness or a decrease in the film thickness. In order to give clarity on this aspect, PEG-free spray-pyrolysis deposition was performed for different layers. Application of 10, 20, 30, and 40 layers of deposition produces films with thicknesses of 340, 415, 610, and 800 nm, respectively (Figure S4a−d in the SI). This reveals a linear proportionality between the deposition layer and film thickness within the range of interest (Figure S4e in the SI), while all films share similar morphology (Figure S5a−d in the SI). Figure S6 in the SI infers the progressive nature of the crystallite density over the thickness increment, similar to that perceived in PEG-assisted films. Furthermore, the absolute absorbance of the films is proportional to their thickness (Figure S7a in the SI), as opposed to their corresponding band

DOI: 10.1021/acsami.5b00853
ACS Appl. Mater. Interfaces 2015, 7, 9088−9097

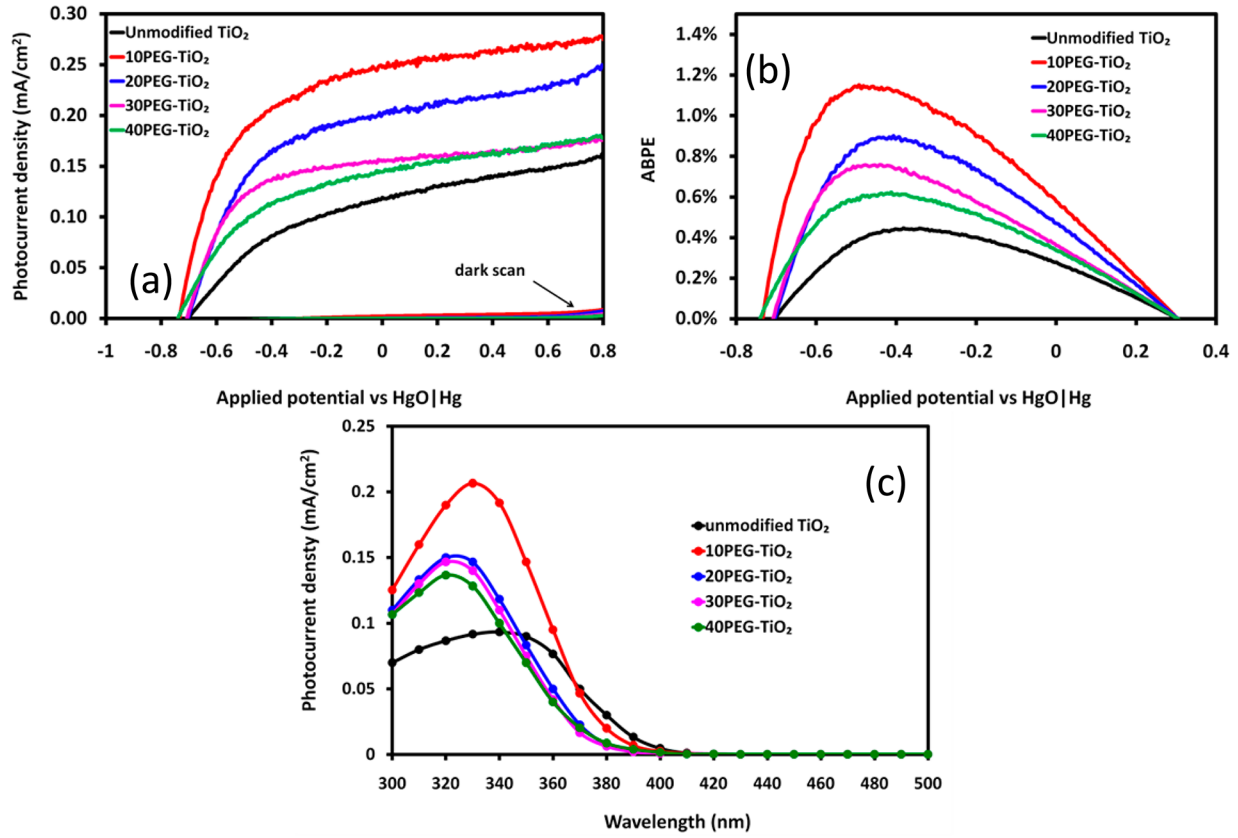

Figure 5. Linear-sweep voltammograms of the synthesized photoanode films (a) along with their corresponding ABPE (b). Photocurrent spectra at 0 V vs HgO|Hg (c).

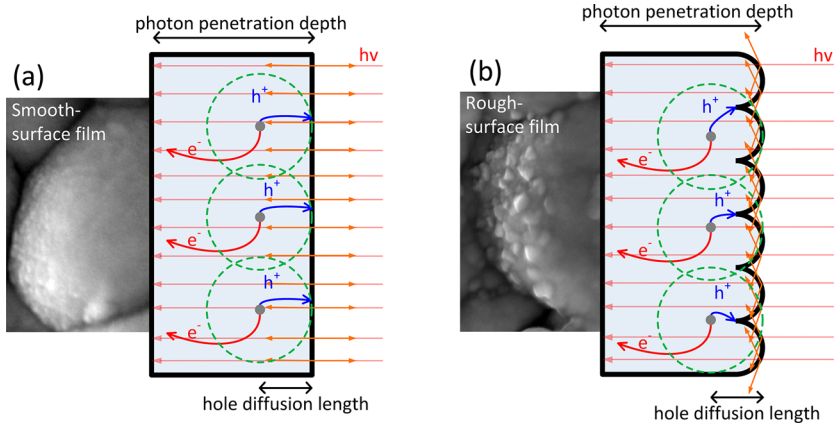

Figure 6. Illustration of light distribution and the hole collection pathway in a smooth-surface film (a) and in a rough-surface film (b).

gaps, which are relatively unaffected by the thickness variation (Figure S7b in the SI). With this information known, Figure 7a illustrates ABPE as a function of the film thickness for two sets of data, i.e., unmodified and PEG-assisted TiO_2 films. Importantly, within a similar range of film thickness, PEG-assisted films give higher PEC efficiency by a significant margin compared to the unmodified ones. This confirms that the PEC enhancement upon PEG addition is governed by the development in the morphology, not by the decrease in the film thickness.

Another important point is depicted in Figure 7b, which compares the maximum ABPE values of unmodified TiO_2 and 10PEG−TiO_2, calculated on the basis of both the geometric and real (effective) surface area. Clearly, when PEC responses are normalized against the real surface area, the differences in the PEC efficiency are not as vast as those observed when PEC responses are normalized against the photon-exposed geometric area. In the case where the effect of the surface area is ruled out by real-area normalization, the improvements are ascribed to roughness-related interfacial phenomena, as previously mentioned. It is therefore important for authors, particularly those who deal with the intrinsic properties of the semiconducting materials in addition to the morphology, to acknowledge the real surface area of their individual films. Otherwise, interpretations on the PEC output will be misleading, and erroneous conclusions may be drawn.

As inferred by experimental observations, PEC responses are not directly proportional to the specific surface area in this

DOI: 10.1021/acsami.5b00853
ACS Appl. Mater. Interfaces 2015, 7, 9088−9097

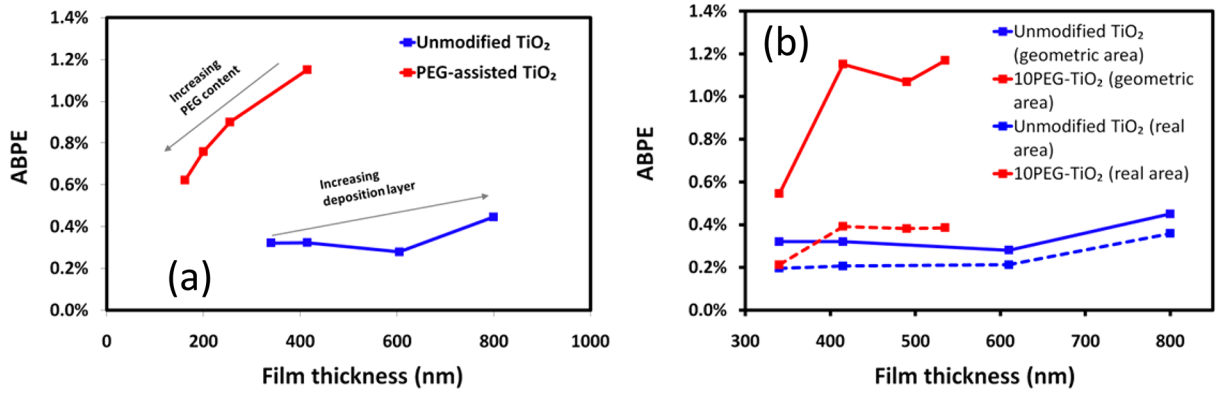

Figure 7. (a) ABPE of the unmodified and PEG-modified TiO_2 films as a function of the film thickness. (b) ABPE of the unmodified TiO_2 and 10PEG−TiO_2 at various thicknesses, calculated on the basis of both the geometric and real surface area.

study. This implies that the PEC activity is not governed solely by the number of reactive sites, and it can be rationalized by considering several aspects. First, as a basis of analysis, one should recall that 10PEG−TiO_2 exhibits not only the highest Sdr value but also the most uniform roughness dispersal (as indicated by the relatively small standard deviation of rms data), thus ensuring high and evenly distributed photokinetics. These attributes of 10PEG−TiO_2 may explain its superior PEC performance compared to that of other films. Second, because 10PEG−TiO_2 is the thickest film among all PEG-assisted samples, it could absorb more photons than its counterparts. Provided that the thickness does not exceed the penetration depth of photons, it is reasonable to expect the PEC performance to be proportional to the film thickness. Besides the fact that it is evident in Figure 7, this hypothesis is particularly true in our system because the values of $1/\alpha$ of the films within the UV region are generally higher than their respective thickness.. Therefore, we believe that photoexcitation occurs within the whole film thickness. This conjecture is even more likely if the possible transitions between the VB and the surface states situated below the CB are taken into account.[21] The degree of crystallization may also play a role. The less-crystalline nature of the films obtained from the solutions with high PEG content is perhaps one of the causes of this negative effect because amorphous regions were reported to hinder carrier transport to some extent.[51,52] Moreover, it was previously revealed that increasing the PEG content leads to higher band gaps. As a result, the thermodynamic photoconversion efficiency decreases,[53] and the photoanodes are prevented from generating higher photocurrents, in spite of their improved morphology. These suggestions should clarify potential confusion with regard to our findings, such as the fact that 40PEG−TiO_2 gives the lowest photoresponses among PEG-assisted films, despite its Sdr value being second only to that of 10-PEG−TiO_2 and its roughness and waviness rms values being the highest among all films.

Figure 8a describes the on−off illumination cycles of the photoanode samples, examined at 0 V vs HgO|Hg (0.926 V vs RHE). As is clearly illustrated, all samples respond instantaneously to light interference, generating a photoanodic current that is orders of magnitude higher than that observed under the dark condition. On the other hand, sudden dark perturbation quickly eliminates the photocurrent, as the photoanodes return to their ground states after several seconds of photoexcitation. Importantly, the stationary photocurrent is restored almost completely in the next few cycles, suggesting the robustness and

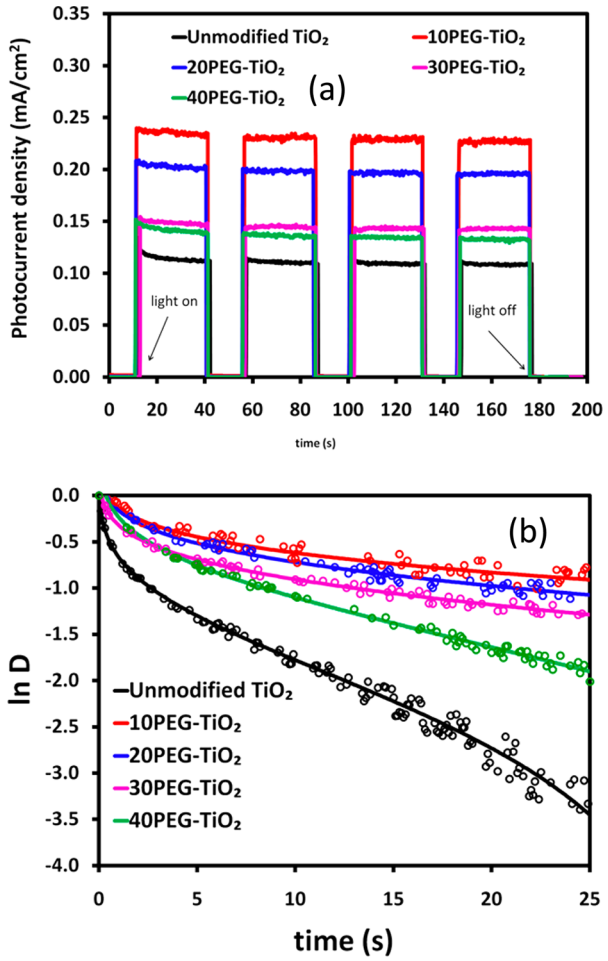

Figure 8. (a) Chronoamperometry of the synthesized films for the on−off illumination mode at 0 V vs HgO|Hg. (b) Time course of ln *D*.

excellent stability of the films. Information concerning the effectiveness of the photocharge transfer can also be drawn from transient photocurrent analysis by deriving time constants (τ) as follows:[42,54−57]

$$D = \frac{j(t) - j(\mathrm{st})}{j(\mathrm{in}) - j(\mathrm{st})} \quad (5)$$

$$D = \exp\left(-\frac{t}{\tau}\right) \rightarrow \ln D = \left(-\frac{1}{\tau}\right)t \quad (6)$$

DOI: 10.1021/acsami.5b00853
ACS Appl. Mater. Interfaces 2015, 7, 9088−9097

Table 1. Selected Reports on TiO_2-Based PEC Water Splitting with Their Respective ABPE Values

photoanodes	preparation method	electrolyte	ABPE (%)	.ref
rough-surface TiO_2 films	PEG-templated spray pyrolysis	1 M NaOH	1.15	this work
cross-linked TiO_2 nanowires	ethylene glycol-mediated	1 M NaOH	1.05	13
Reduced TiO_2 nanotube arrays	anodization, $NaBH_4$ treatment	1 M NaOH	1.31	58
TiO_2 nanospider films	PEG-templated	0.1 M NaOH	0.23	37
TiO_2 nanorod arrays	oblique-angle deposition	0.5 M $NaClO_4$	0.10	59
UV−vis TiO_2 double layer	radio-frequency magnetron sputtering	0.25 M K_2SO_4	0.17	60
TiO_2 nanotube arrays	anodization, flame annealing	1 M KOH	1.20	61
3D hierarchical TiO_2 nanostructured arrays	hydrothermal on seeded FTO	1 M KOH	1.13	45
H_2-treated TiO_2 nanowire arrays	hydrothermal and H_2 annealing	1 M NaOH	1.63	15
TiO_2 nanoporous arrays	Anodization	1 M KOH	0.28	62
Sn-doped TiO_2 nanorods	Hydrothermal	1 M KOH	0.69	17
Au-SPR-enhanced TiO_2 films	template-assisted sol−gel	1 M KOH	0.71	63
TiO_2 nanotube arrays	anodization	0.5 M $NaClO_4$, 0.5 M $HClO_4$ and 1 M NaOH	0.27	64
Sn-doped TiO_2 nanowire arrays	hydrothermal	1 M KOH	1.20	65
hierarchical TiO_2 nanotube arrays	two-step anodization	1 M KOH	0.84	46
N-doped double-wall TiO_2 nanotube array	two-step anodization	1 M KOH	1.26	66
branched TiO_2 nanorods	hydrothermal	1 M KOH	0.49	16

where $j(t)$ is the photocurrent at time t, j(st) is the stationary photocurrent, and j(in) is the initial photocurrent. Figure 8b depicts the plots of ln D against the illumination time for all prepared samples. The decline of ln D over time is ascribed to the undesired recombination of charge carriers on the surface.[54] Linearity of these decays is expected if the resistance of photocharge transport is driven by first-order kinetics,[54] in which case τ can be directly calculated from the negative inverse of the slope (eq 6). More complex decay mechanisms entail deviation from linearity.[54] This nonlinearity is observed in Figure 8b to an extent where extracting τ with acceptable R^2 values is not possible. Nonetheless, in order to give qualitative insight, one can still notice the apparent variance in the drop rate of ln D between all films, inferring more efficient photocharge transport in the case of PEG-assisted films.

Comprehensive analysis of a PEC system can be performed by considering three fundamental processes governing its overall efficiency,[47] i.e., photocharge extraction upon photoinduction (the efficiency of which is denoted by η_{e^-/h^+}), transport of these photogenerated charges ($\eta_{transport}$), and interfacial redox reactions ($\eta_{interface}$). The overall efficiency of PEC water splitting can then be expressed as[47]

$$\eta_{overall} = \eta_{e^-/h^+}\eta_{transport}\eta_{interface} \quad (7)$$

We mentioned earlier that unmodified TiO_2 is the thickest among all films, yet it should be emphasized that its thickness is still within the effective region of photon penetration. Consequently, it is expected that unmodified TiO_2 possesses the highest value of η_{e^-/h^+} in the sense that more excitons are generated with the same amount of incident photons impinging on the photoanode. Despite this suggestion, however, the PEG-modified films outperform their unmodified counterparts during PEC operations. This indicates that, upon morphological modification, the significance of η_{e^-/h^+} on $\eta_{overall}$ is marginalized compared to that of $\eta_{interface}$ and $\eta_{transport}$. In typical PEC studies, the PEC behavior of photoanode materials is normalized against the illuminated geometric area of the photoanodes. Consequently, extensions of the effective surface area and/or improvements in interfacial phenomena due to surface roughening will boost $\eta_{interface}$. Furthermore, one should consider the interrelationship between $\eta_{transport}$ and $\eta_{interface}$, which is perhaps advantageous in our PEC system. On the one hand, the high rate consumption of photocharges at the interface can only be in effect if $\eta_{transport}$ is substantial enough to separate electron−hole pairs and drive the holes approaching the surface. On the other hand, if $\eta_{interface}$ is high enough to promptly quench the VB holes, the electroneutrality principle necessitates that the CB electrons be driven away from the surface, hence improving $\eta_{transport}$, provided that electron acceptors are absent both on the surface and in the electrolyte. In any case, it should be noted that morphological modification is a crucial strategy in order to advance the performance of titania-based PEC systems, as is evident in the present study.

Table 1 collates a list of selected reports on TiO_2-based PEC water splitting and their corresponding ABPE under broad-spectrum illumination. It is clear that the PEC performance of our films is comparable to those of other notable TiO_2-based films. One should note that ABPE is by no means decisive to claim superiority of a particular photoanode against others. While the proper benchmark should be performed on the basis of solar-to-H_2 (STH) efficiency,[47] it involves zero-bias operation and/or accurate detection of evolved H_2 gas in the cell, which is not a simple task in most PEC experimental setups. Nonetheless, because ABPE takes into account the effects of electrical bias and is normalized against the light power density, a comparison between reported works can still be performed in a sensible manner, and ABPE remains a reliable diagnostic approach[47] upon which the development of photoanode materials is based.

4. CONCLUSIONS AND REMARKS

TiO_2 films with tailored morphology can be synthesized via a facile and simple spray-pyrolysis method in the presence of PEG in precursor solutions. PEG plays an important role as a templating agent and successfully improves the roughness and real surface area of photoanode films. The rough-surface films may offer a combination of beneficial features, e.g., increasing interfacial reactive sites for the interaction between photocharges and their redox pairs, intensifying reactant adsorption on the material surface, promoting light scattering for better photon distribution, and/or shortening the hole collection pathways for faster carrier transfer. The concentration of PEG also strongly affects the film thickness. However, the experimental results confirm that enhancements in PEC

DOI: 10.1021/acsami.5b00853
ACS Appl. Mater. Interfaces 2015, 7, 9088−9097

responses are governed predominantly by the film morphology. From this study, it is also suggested that normalizing the PEC output against the real surface area, rather than the geometric area, is a matter of importance, particularly when the intrinsic properties of the photoanode films are to be evaluated. The best PEG-assisted TiO_2 photoanode in this study managed to achieve a photoconversion efficiency of 1.15%, which is comparable to those of other notable reports on titania-based PEC systems.

■ ASSOCIATED CONTENT

Supporting Information

SEM images of the FTO substrate, unmodified TiO_2 film, and 10PEG−TiO_2 film with different deposition layers, XRD patterns of the unmodified TiO_2 film with different deposition layers, TEM images and energy-dispersive spectra of the unmodified TiO_2 and 10PEG−TIO_2 films, UV−vis absorbance spectra of the unmodified TiO_2 film with different deposition layers, and PEC performances of unmodified TiO_2 and 10PEG−TiO_2 with different deposition layers. This material is available free of charge via the Internet at http://pubs.acs.org.

■ AUTHOR INFORMATION

Corresponding Author

*Tel: +44 (0)20 7594 5577. E-mail: k.hellgardt@imperial.ac.uk.

Notes

The authors declare no competing financial interest.

■ ACKNOWLEDGMENTS

This research is supported by the Directorate General of Higher Education (DIKTI), Indonesian Ministry of Education and Culture, via a doctoral scholarship for M.I. (568/E4.4/K/2012).

■ REFERENCES

(1) Holladay, J. D.; Hu, J.; King, D. L.; Wang, Y. An Overview of Hydrogen Production Technologies. *Catal. Today* **2009**, *139*, 244−260.

(2) Turner, J.; Sverdrup, G.; Mann, M. K.; Maness, P.-C.; Kroposki, B.; Ghirardi, M.; Evans, R. J.; Blake, D. Renewable Hydrogen Production. *Int. J. Energy Res.* **2008**, *32*, 379−407.

(3) Fujishima, A.; Honda, K. Electrochemical Photolysis of Water at a Semiconductor Electrode. *Nature* **1972**, *238*, 37−38.

(4) Lianos, P. Production of Electricity and Hydrogen by Photocatalytic Degradation of Organic Wastes in a Photoelectrochemical Cell: The Concept of the Photofuelcell: A Review of a Re-Emerging Research Field. *J. Hazard. Mater.* **2011**, *185*, 575−590.

(5) Osterloh, F. E.; Parkinson, B. A. Recent Developments in Solar Water-Splitting Photocatalysis. *MRS Bull.* **2011**, *36*, 17−22.

(6) Currao, A. Photoelectrochemical Water Splitting. *CHIMIA Int. J. Chem.* **2007**, *61*, 815−819.

(7) Liu, Z.; Sun, D. D.; Guo, P.; Leckie, J. O. An Efficient Bicomponent TiO_2/SnO_2 Nanofiber Photocatalyst Fabricated by Electrospinning with a Side-by-Side Dual Spinneret Method. *Nano Lett.* **2006**, *7*, 1081−1085.

(8) Butterfield, I. M.; Christensen, P. A.; Hamnett, A.; Shaw, K. E.; Walker, G. M.; Walker, S. A.; Howarth, C. R. Applied Studies on Immobilized Titanium Dioxide Films as Catalysts for the Photoelectrochemical Detoxification of Water. *J. Appl. Electrochem.* **1997**, *27*, 385−395.

(9) Palmas, S.; Da Pozzo, A.; Delogu, F.; Mascia, M.; Vacca, A.; Guisbiers, G. Characterization of TiO_2 Nanotubes Obtained by Electrochemical Anodization in Organic Electrolytes. *J. Power Sources* **2012**, *204*, 265−272.

(10) Mohapatra, S. K.; Misra, M.; Mahajan, V. K.; Raja, K. S. Design of a Highly Efficient Photoelectrolytic Cell for Hydrogen Generation by Water Splitting: Application of TiO_2−XC_x Nanotubes as a Photoanode and Pt/TiO_2 Nanotubes as a Cathode. *J. Phys. Chem. C* **2007**, *111*, 8677−8685.

(11) Paulose, M.; Shankar, K.; Yoriya, S.; Prakasam, H. E.; Varghese, O. K.; Mor, G. K.; Latempa, T. A.; Fitzgerald, A.; Grimes, C. A. Anodic Growth of Highly Ordered TiO_2 Nanotube Arrays to 134 μm in Length. *J. Phys. Chem. B* **2006**, *110*, 16179−16184.

(12) Slamet; Tristantini, D.; Valentina; Ibadurrohman, M. Photocatalytic Hydrogen Production from Glycerol−Water Mixture over Pt-N-TiO_2 Nanotube Photocatalyst. *Int. J. Energy Res.* **2013**, *37*, 1372−1381.

(13) Liu, M.; de Leon Snapp, N.; Park, H. Water Photolysis with a Cross-Linked Titanium Dioxide Nanowire Anode. *Chem. Sci.* **2011**, *2*, 80−87.

(14) Hoang, S.; Guo, S.; Hahn, N. T.; Bard, A. J.; Mullins, C. B. Visible Light Driven Photoelectrochemical Water Oxidation on Nitrogen-Modified TiO_2 nanowires. *Nano Lett.* **2012**, *12*, 26−32.

(15) Wang, G.; Wang, H.; Ling, Y.; Tang, Y.; Yang, X.; Fitzmorris, R. C.; Wang, C.; Zhang, J. Z.; Li, Y. Hydrogen-Treated TiO_2 Nanowire Arrays for Photoelectrochemical Water Splitting. *Nano Lett.* **2011**, *11*, 3026−3033.

(16) Cho, I.; Chen, Z.; Forman, A.; Kim, D.; Rao, P.; Jaramillo, T.; Zheng, X. Branched TiO_2 Nanorods for Photoelectrochemical Hydrogen Production. *Nano Lett.* **2011**, *11*, 4978−4984.

(17) Sun, B.; Shi, T.; Peng, Z.; Sheng, W.; Jiang, T.; Liao, G. Controlled Fabrication of Sn/TiO_2 Nanorods for Photoelectrochemical Water Splitting. *Nanoscale Res. Lett.* **2013**, *8*, 462.

(18) Liu, C.; Li, Y.; Wei, L.; Wu, C.; Chen, Y.; Mei, L.; Jiao, J. Cds Quantum Dot-Sensitized Solar Cells Based on Nano-Branched TiO_2 Arrays. *Nanoscale Res. Lett.* **2014**, *9*, 107.

(19) Oh, J.; Lee, J.; Kim, H.; Han, S.; Park, K. TiO_2 Branched Nanostructure Electrodes Synthesized by Seeding Method for Dye-Sensitized Solar Cells. *Chem. Mater.* **2010**, *22*, 1114−1118.

(20) Osterloh, F. E. Inorganic Nanostructures for Photoelectrochemical and Photocatalytic Water Splitting. *Chem. Soc. Rev.* **2013**, *42*, 2294−2320.

(21) Pu, P.; Cachet, H.; Ngaboyamahina, E.; Sutter, E. M. M. Relation between Morphology and Conductivity in TiO_2 Nanotube Arrays: An Electrochemical Impedance Spectrometric Investigation. *J. Solid State Electrochem.* **2013**, *17*, 817−828.

(22) Kajihara, K.; Nakanishi, K.; Tanaka, K.; Hirao, K.; Soga, N. Preparation of Macroporous Titania Films by a Sol−Gel Dip-Coating Method from the System Containing Poly(Ethylene Glycol). *J. Am. Ceram. Soc.* **1998**, *81*, 2670−2676.

(23) Liau, L. C.-K.; Chang, H.; Yang, T. C.-K.; Huang, C.-L. Effect of Poly(Ethylene Glycol) Additives on the Photocatalytic Activity of TiO_2 Films Prepared by Sol−Gel Processing and Low Temperature Treatments. *J. Chin. Inst. Chem. Eng.* **2008**, *39*, 237−242.

(24) Bu, S.; Jin, Z.; Liu, X.; Yang, L.; Cheng, Z. Fabrication of TiO_2 Porous Thin Films Using Peg Templates and Chemistry of the Process. *Mater. Chem. Phys.* **2004**, *88*, 273−279.

(25) Bu, S. J.; Jin, Z. G.; Liu, X. X.; Yang, L. R.; Cheng, Z. J. Synthesis of TiO_2 Porous Thin Films by Polyethylene Glycol Templating and Chemistry of the Process. *J. Eur. Ceram. Soc.* **2005**, *25*, 673−679.

(26) Arconada, N.; Durán, A.; Suárez, S.; Portela, R.; Coronado, J. M.; Sánchez, B.; Castro, Y. Synthesis and Photocatalytic Properties of Dense and Porous TiO_2−Anatase Thin Films Prepared by Sol−Gel. *Appl. Catal. B: Environ.* **2009**, *86*, 1−7.

(27) Arpi, M.; Subhayan, B.; Faruk, H. M.; Takakazu, T. Study of Gradual Variation of Structural, Surface Morphological and Photocatalytic Properties of Sol−Gel Derived Transparent Tio2 Thin Film. *J. Phys.: Conf. Ser.* **2008**, *100*, 012006.

(28) Guo, B.; Liu, Z.; Hong, L.; Jiang, H. Sol Gel Derived Photocatalytic Porous TiO_2 Thin Films. *Surf. Coat. Technol.* **2005**, *198*, 24−29.

DOI: 10.1021/acsami.5b00853
ACS Appl. Mater. Interfaces 2015, 7, 9088−9097

(29) Sabataitytė, J.; Oja, I.; Lenzmann, F.; Volobujeva, O.; Krunks, M. Characterization of Nanoporous TiO_2 Films Prepared by Sol−Gel Method. *C. R. Chimie* **2006**, *9*, 708−712.
(30) Tan, R.; He, Y.; Zhu, Y.; Xu, B.; Cao, L. Hydrothermal Preparation of Mesoporous TiO_2 Powder from $Ti(SO_4)_2$ with Poly(Ethylene Glycol) as Template. *J. Mater. Sci.* **2003**, *38*, 3973−3978.
(31) de Tacconi, N. R.; Chenthamarakshan, C. R.; Yogeeswaran, G.; Watcharenwong, A.; de Zoysa, R. S.; Basit, N. A.; Rajeshwar, K. Nanoporous TiO_2 and WO_3 Films by Anodization of Titanium and Tungsten Substrates: Influence of Process Variables on Morphology and Photoelectrochemical Response. *J. Phys. Chem. B* **2006**, *110*, 25347−25355.
(32) Uzunova-Bujnova, M.; Todorovska, R.; Milanova, M.; Kralchevska, R.; Todorovsky, D. On the Spray-Drying Deposition of TiO_2 Photocatalytic Films. *Appl. Surf. Sci.* **2009**, *256*, 830−837.
(33) Choy, K. L.; Su, B. Titanium Dioxide Anatase Thin Films Produced by Electrostatic Spray Assisted Vapor Deposition (Esavd) Technique. *J. Mater. Sci. Lett.* **1999**, *18*, 943−945.
(34) Huang, W.; Lei, M.; Huang, H.; Chen, J.; Chen, H. Effect of Polyethylene Glycol on Hydrophilic TiO_2 Films: Porosity-Driven Superhydrophilicity. *Surf. Coat. Technol.* **2010**, *204*, 3954−3961.
(35) Jo, E. H.; Chang, H.; Kim, S. K.; Roh, K. M.; Kim, J.; Jang, H. D. Pore Size-Controlled Synthesis of PEG-Derived Porous TiO_2 Particles and Photovoltaic Performance of Dye-Sensitized Solar Cells. *Mater. Lett.* **2014**, *131*, 244−247.
(36) Ramírez-Santos, Á. A.; Acevedo-Peña, P.; Córdoba, E. M. Enhanced Photocatalytic Activity of TiO_2 Films by Modification with Polyethylene Glycol. *Quim. Nova* **2012**, *35*, 1931−1935.
(37) Fei, H.; Yang, Y.; Rogow, D. L.; Fan, X.; Oliver, S. R. J. Polymer-Templated Nanospider TiO_2 Thin Films for Efficient Photoelectrochemical Water Splitting. *ACS Appl. Mater. Interfaces* **2010**, *2*, 974−979.
(38) Turner, J. A. A Realizable Renewable Energy Future. *Science* **1999**, *285*, 687−689.
(39) Xue, X.; Ji, W.; Mao, Z.; Mao, H.; Wang, Y.; Wang, X.; Ruan, W.; Zhao, B.; Lombardi, J. R. Raman Investigation of Nanosized TiO_2: Effect of Crystallite Size and Quantum Confinement. *J. Phys. Chem. C* **2012**, *116*, 8792−8797.
(40) Yu, J.; Zhao, X.; Zhao, Q. Effect of Film Thickness on the Grain Size and Photocatalytic Activity of the Sol−Gel Derived Nanometer TiO_2 Thin Films. *J. Mater. Sci. Lett.* **2000**, *19*, 1015−1017.
(41) Tauc, J. Optical Properties and Electronic Structure of Amorphous Ge and Si. *Mater. Res. Bull.* **1968**, *3*, 37−46.
(42) Radecka, M.; Rekas, M.; Trenczek-Zajac, A.; Zakrzewska, K. Importance of the Band Gap Energy and Flat Band Potential for Application of Modified TiO_2 Photoanodes in Water Photolysis. *J. Power Sources* **2008**, *181*, 46−55.
(43) Tian, G.-L.; He, H.-B.; Shao, J.-D. Effect of Microstructure of TiO_2 Thin Films on Optical Band Gap Energy. *Chin. Phys. Lett.* **2005**, *22*, 1787.
(44) Lee, S.; Cho, I.-S.; Noh, J.-H.; Hong, K. S.; Han, G. S.; Jung, H. S.; Jeong, S.; Lee, C.; Shin, H. Correlation of Anatase Particle Size with Photocatalytic Properties. *Phys. Status Solidi A* **2010**, *207*, 2288−2291.
(45) Yang, J.-S.; Liao, W.-P.; Wu, J.-J. Morphology and Interfacial Energetics Controls for Hierarchical Anatase/Rutile TiO_2 Nanostructured Array for Efficient Photoelectrochemical Water Splitting. *ACS Appl. Mater. Interfaces* **2013**, *5*, 7425−7431.
(46) Zhang, Z.; Wang, P. Optimization of Photoelectrochemical Water Splitting Performance on Hierarchical TiO_2 Nanotube Arrays. *Energy Environ. Sci.* **2012**, *5*, 6506−6512.
(47) Chen, Z.; Dinh, H.; Miller, E. Photoelectrochemical Water Splitting. In *Standards, Experimental Methods, and Protocols [Online]*; Springer: New York, 2013.
(48) Takahashi, M.; Tsukigi, K.; Uchino, T.; Yoko, T. Enhanced Photocurrent in Thin Film TiO_2 Electrodes Prepared by Sol−Gel Method. *Thin Solid Films* **2001**, *388*, 231−236.
(49) Nozik, A. J.; Miller, J. Introduction to Solar Photon Conversion. *Chem. Rev.* **2010**, *110*, 6443−6445.
(50) Rees, N. V.; Compton, R. G. Carbon-Free Energy: A Review of Ammonia- and Hydrazine-Based Electrochemical Fuel Cells. *Energy Environ. Sci.* **2011**, *4*, 1255−1260.
(51) Eufinger, K.; Poelman, D.; Poelman, H.; Gryse, R. D.; Marin, G. B. Effect of Microstructure and Crystallinity on the Photocatalytic Activity of TiO_2 Thin Films Deposited by Dc Magnetron Sputtering. *J. Phys. D: Appl. Phys.* **2007**, *40*, 5232.
(52) Tanaka, K.; Capule, M. F. V.; Hisanaga, T. Effect of Crystallinity of TiO_2 on Its Photocatalytic Action. *Chem. Phys. Lett.* **1991**, *187*, 73−76.
(53) Murphy, A. B.; Barnes, P. R. F.; Randeniya, L. K.; Plumb, I. C.; Grey, I. E.; Horne, M. D.; Glasscock, J. A. Efficiency of Solar Water Splitting Using Semiconductor Electrodes. *Int. J. Hydrogen Energy* **2006**, *31*, 1999−2017.
(54) Hagfeldt, A.; Lindström, H.; Södergren, S.; Lindquist, S.-E. Photoelectrochemical Studies of Colloidal TiO_2 Films: The Effect of Oxygen Studied by Photocurrent Transients. *J. Electroanal. Chem.* **1995**, *381*, 39−46.
(55) Radecka, M.; Wierzbicka, M.; Komornicki, S.; Rekas, M. Influence of Cr on Photoelectrochemical Properties of TiO_2 Thin Films. *Physica B: Condensed Matter* **2004**, *348*, 160−168.
(56) Ng, Y. H.; Iwase, A.; Kudo, A.; Amal, R. Reducing Graphene Oxide on a Visible-Light $BiVO_4$ Photocatalyst for an Enhanced Photoelectrochemical Water Splitting. *J. Phys. Chem. Lett.* **2010**, *1*, 2607−2612.
(57) Bell, N. J.; Ng, Y. H.; Du, A.; Coster, H.; Smith, S. C.; Amal, R. Understanding the Enhancement in Photoelectrochemical Properties of Photocatalytically Prepared TiO_2-Reduced Graphene Oxide Composite. *J. Phys. Chem. C* **2011**, *115*, 6004−6009.
(58) Kang, Q.; Cao, J.; Zhang, Y.; Liu, L.; Xu, H.; Ye, J. Reduced TiO_2 Nanotube Arrays for Photoelectrochemical Water Splitting. *J. Mater. Chem. A* **2013**, *1*, 5766−5774.
(59) Wolcott, A.; Smith, W. A.; Kuykendall, T. R.; Zhao, Y.; Zhang, J. Z. Photoelectrochemical Water Splitting Using Dense and Aligned TiO_2 Nanorod Arrays. *Small* **2009**, *5*, 104−111.
(60) Tode, R.; Ebrahimi, A.; Fukumoto, S.; Iyatani, K.; Takeuchi, M.; Matsuoka, M.; Lee, C.; Jiang, C.-S.; Anpo, M. Photocatalytic Decomposition of Water on Double-Layered Visible Light-Responsive TiO_2 Thin Films Prepared by a Magnetron Sputtering Deposition Method. *Catal. Lett.* **2010**, *135*, 10−15.
(61) Mazare, A.; Paramasivam, I.; Lee, K.; Schmuki, P. Improved Water-Splitting Behaviour of Flame Annealed TiO_2 Nanotubes. *Electrochem. Commun.* **2011**, *13*, 1030−1034.
(62) Liu, Y.; Zhou, B.; Bai, J.; Li, J.; Zhang, J.; Zheng, Q.; Zhu, X.; Cai, W. Efficient Photochemical Water Splitting and Organic Pollutant Degradation by Highly Ordered TiO_2 Nanopore Arrays. *Appl. Catal. B: Environ.* **2009**, *89*, 142−148.
(63) Zhang, X.; Liu, Y.; Lee, S.-T.; Yang, S.; Kang, Z. Coupling Surface Plasmon Resonance of Gold Nanoparticles with Slow-Photon-Effect of TiO_2 Photonic Crystals for Synergistically Enhanced Photoelectrochemical Water Splitting. *Energy Environ. Sci.* **2014**, *7*, 1409−1419.
(64) Kong, D.-S.; Wei, Y.-J.; Li, X.-X.; Zhang, Y.; Feng, Y.-Y.; Li, W.-J. pH Dependent Behavior and Effects of Photoinduced Surface States During Water Photooxidation at TiO_2/Solution Interface: Studied by Capacitance Measurements. *J. Electrochem. Soc.* **2014**, *161*, H144−H153.
(65) Xu, M.; Da, P.; Wu, H.; Zhao, D.; Zheng, G. Controlled Sn-Doping in TiO_2 Nanowire Photoanodes with Enhanced Photoelectrochemical Conversion. *Nano Lett.* **2012**, *12*, 1503−1508.
(66) Wu, H.; Zhang, Z. High Photoelectrochemical Water Splitting Performance on Nitrogen Doped Double-Wall TiO_2 Nanotube Array Electrodes. *Int. J. Hydrogen Energy* **2011**, *36*, 13481−13487.

DOI: 10.1021/acsami.5b00853
ACS Appl. Mater. Interfaces 2015, 7, 9088−9097